Geosci. Instrum. Method. Data Syst. Discuss., 3, 1–30, 2013
www.geosci-instrum-method-data-syst-discuss.net/3/1/2013/
doi:10.5194/gid-3-1-2013

Geoscientific Instrumentation Methods and Data Systems Discussions

Possible application of a compact electronics for multilayer muon high-speed radiography to volcanic cones

H. K. M. Tanaka[1] **and I. Yokoyama**[2]

[1]Earthquake Research Institute, the University of Tokyo, Tokyo, Japan
[2]The Japan Academy, Tokyo, Japan

Received: 27 August 2012 – Accepted: 28 November 2012 – Published: 21 January 2013

Correspondence to: H. K. M. Tanaka (ht@riken.jp)

Published by Copernicus Publications on behalf of the European Geosciences Union.

Abstract

A compact data taking electronics was developed for high-speed multi-layer muon radiography in order to minimize the operation failure rate. By requesting a linear trajectory within the number of redundant position sensitive detectors (PSDs), the background (BG) events produced by vertical electromagnetic (EM) showers are effectively reduced. In order to confirm the feasibility of this method, the system comprising 4 PSD layers were tested by imaging the internal structure of a parasitic cone and the adjacent craterlets formed in the 1910 eruption at the base of Usu volcano, Hokkaido with a conventional (MURG08) readout system (Kusagaya et al., 2012; Tanaka et al., 2012). The new mountain has been believed to be a cryptodome since its formation. According As knowledge on lava domes is are accumulated at various volcanoes, the definition of "cryptodome" is now doubted in its validity. The results of the preliminary 290-h muon radiographic survey revealed that the "cryptodome" is not underlain by any lava mass and that a main craterlet is accompanied by magma intrusions at shallow depths. The former verifies that the new mountain is not a cryptodome but a volcanogenetic mound, and the latter interprets the phreatic explosions forming the craterlets as intrusions of magma into the aquifer. However, a higher data taking failure rate was observed with a software-based MURG08 system when the size of the active area of the detection system was enlarged to improve the detection ability of the system. The newly developed MURG12 is a complete hardware-based electronics system that can simultaneously process signals from 192 scintillation counters of data size of 600 kbps ch^{-1} without operation failure. We anticipate that the observation speed would be further improved by employing MURG12.

At the base of Usu volcano, in 20th century, four eruptions occurred. Some of them demonstrated three characteristic magma intrusions. First, a magma branch remained at a depth leaving an upheaval of the ground, second, it rose and reached aquifers causing phreatic explosions but not extruded, and third, it reacted with aquifers causing phreatic explosions and further extruded over the ground forming a lava dome. In order

GID

3, 1–30, 2013

to clarify the eruption mechanism of Usu, it is necessary for us to image many parasitic cones. Based on the result of the test measurement, we anticipate that MURG12 would be a strong tool for high-speed muon radiography.

1 Introduction

Muon radiography was first introduced to volcanology in 2006 at Asama volcano by Tanaka et al. (2007a) and succeeded in imaging displacements of volcanic material within the summit crater (Tanaka et al., 2009). Striking examples of the success in imaging of internal structure of volcanic edifices are seen on Japanese volcanoes. Merits of the muon radiography are ability of remote sensing, high resolution, possibly to reconstruct tomographic images accuracy due to tomography, by combining the cosmic-ray muon energy spectrum and the relationship between the muon energy and the stopping power. Muon radiography was first proposed to determine a thickness of an overburden of a horizontal tunnel in the Snowy Mountains in Australia (George, 1955). He measured the muon flux inside and outside the tunnel to compare them to confirm that a reduction in the muon flux reflects the average density of the overburden. The comparison of the muon flux measured inside and outside the tunnel confirmed that the reduction in the muon flux reflects the average density of the rock overburden. In 1969, he applied George's idea was applied to the "Great Pyramid" of Giza to search for undiscovered chambers (Alvarez et al., 1970).

Interactions of primary cosmic rays with the earth's atmosphere produce a flux of high energy muons. These muons come mostly from the vertical, following a known zenith angular distribution. It is also known that muons are arriving in the horizontal direction with a smaller average intensity, but with a higher intensity at energies above a few 100 GeV. These horizontal muons can be used to perform for radiography of a volcano. If the topography of a volcano is known, the information from counting muon events in the detector at different arriving angles can be used to infer the average density of the matter through which the muons traveled because only the integrated

GID
3, 1–30, 2013

effect along the travel path leads to the attenuation of the flux. Since most muon cannot penetrate more than a few km through solid material, the target is limited to the top region or a small volcano. However, the spatial resolution of the image is better than the one obtained by higher than the seismic tomography.

Since then, Muon radiography has achieved interesting results on several volcanoes such as Usu (Tanaka and Yokoyama, 2008), Asama (Tanaka et al., 2007, 2009a, 2010), Satsuma-Iwo-jima (Tanaka et al., 2009b) and other volcanoes (Lesparre et al., 2012). At the same time, the technique itself has been advanced rapidly.

The high penetration depth of muons in matter enables studies of the internal structure of geological formations. However, as the muon path length becomes longer, the penetrating muon flux substantially decreases. Therefore, the high BG rate substantially degrades the time resolution of the technique. The most probable source of the BG is the simultaneously arriving vertical electromagnetic (EM) shower that includes high energy muons, electrons, positrons, and gamma rays. The EM shower hits random points in the position sensitive detectors (PSDs) simultaneously.

When the EM shower particles hit more than one points on the PSD, the multiplicity hit analysis is effective as reported by Tanaka et al. (2001). However, when the EM shower hits only one point on each PSD, a system comprising two PSD layers can create a fake muon track. If we insert a redundant PSD between two PSDs, we can request a linear trajectory for a muon event. The possibility for the EM shower to make a linear trajectory is further reduced if we insert two or more redundant PSDs.

If we lower the BG rate, the time required for distinguishing a density contrast is generally shortened. The reason is described as follows. In order to detect the variations in the penetrating muon flux (ΔN), it is required for us to wait until the variations are larger than the statistical fluctuations in the number of recorded events: it is required for us to wait until $\Delta N > \sqrt{N} + \Delta N_{\mathrm{BG}}$, where N is the number of true muon events that is assumed to tend towards a Poisson process in the limit of very high seizes, and ΔN_{BG} is the number of the BG events from the fake tracks. Larger the background contamination, larger the observation time is required to be. This ΔN_{BG} extends the necessary

GID
3, 1–30, 2013

observation time. For example, the times required to resolve density fluctuation of 10 % through rock with a thickness of 1 km water equivalent (kmwe) at 1σ confidence level (CL) will be extended by factors of 3.7 and 6 when $\Delta N_{BG} = 0.5N$ and when $\Delta N_{BG} = N$, respectively.

In 2007, density distribution of 1944 Usu lava dome (Tanaka et al., 2007) was measured with muon radiography. Considering the typical thickness of ~ 500 m of the target volume, the muon intensity of 3000/sr/day is expected. The data, however, contains significant amount of background, and therefore, it took 120 days to resolve the internal structure. The multi-layer muon detection system would give the density distribution of the similar target much faster.

Muon radiography is most effectively applicable to volcanic edifices of linear dimension $1 \sim 5$ km.w.e (water equivalent). Suitable objects are explosion craters at summits, conduit parts near summit, isolated domes and mounds on summits or slopes of volcanoes. By these observations, we may clarify material supply in the active craters; magmatic activities along conduits (sometimes magma stops); and subsurface magma movements in case of progressing dome formations. High-speed muon radiography system would be ideal to study copious amounts of parasitic cones and domes.

In this work, a hardware-based 196-channel readout module called MURG12 was developed. The board can simultaneously process signals from 192 scintillation counters at a rate of 600 kbps ch^{-1} process the signal input of 192 ch $\times$ 1 MHz ch^{-1} without operation failures. The possible targets will be discussed based on a test measurement with MURG08.

2 Observation system

Conventional multi layer muon radiography has been performed by utilizing MURG08 module developed by Uchida et al. (2009) (Kusagaya et al., 2012). Although the function of "X-Y coincidence checker" is equipped on MURG08 module, the "inter-plane coincidence checking" was carried out on the DAQ PC. As a result, when the event

GID
3, 1–30, 2013

rate (the data transfer rate) increased, the processor overload occurred and as a result, the operation failure can happen.

A block diagram of the multi-layer muon detection system is shown in Fig. 1. The system consists of two major parts – the multilayer PSD module and the readout module. The multilayer PSD module is described in detail somewhere else (Kusagaya et al., 2012) and only is briefly described here. The PSD contains scintillator strips arranged along the x and y coordinates like a lattice. The size of one lattice is $10 \times 10\,\mathrm{cm}^2$. The x-plane and y-plane detect the horizontal and vertical crossing position of a muon, respectively. There are 14 readout channels for each plane. The readout module processes signals from the PSDs and generates the path information that is described in the following paragraphs a histogram for an angular resolution. For communication between the readout module and the data taking computer located at a remote observation station, a wired or wireless local area network (LAN) can be employed. The readout module plays a central role in this system and is discussed in detail in this section.

MURG12 readout module consists of a main board and 10 daughter boards, that are which is $305 \times 235 \times 60\,\mathrm{mm}^3$ each in size. Figure 2 shows a photograph of the main board and a schematic side view of the daughter board. The daughter board mounted on the main board plays a role as a signal filter and comparators as well as a connector adapter so as to allow the use of various types of connectors. Each The daughter board has a shape of a slot card. As shown in Fig. 2, the main board has 10 pairs of slots for daughter boards (the daughter board uses two slots). Each daughter board has 20 LEMO connectors (taken from the engineer's name Léon Mouttet), a signal filter, and a comparator. A signal filter consists of transient voltage suppression (TVS) array to prevent damage to the main board from an accidental large current. The maximum acceptable charge is 10 nC (±100 V within 50 ns). The detector signals are received by the comparators and are digitized after they have been compared with threshold voltage. The threshold voltage is adjustable from −1000 mV to +50 mV. The minimum acceptable pulse width is 5 ns. The digitized signals are processed by the main board,

GID
3, 1–30, 2013

and the main parts of this board are a field programmable gate array (FPGA) (Xilinx Spartan-6FPGA) and an Ethernet physical layer device (PHY). Figure T3 shows a block diagram of the readout module that consists of LEMO connectors, a signal filter, comparators, an event filter, a network processor, and an Ethernet PHY. The event filter, the histogram generator, and the network processor are implemented on the single FPGA.

The event filter selects candidate muon events for which the muon path can be constructed and generates information data on the paths. The signals from 14 x and y-planes that consists of 196 scintillator strips can be processed on the single FPGA. It is shown as "14 input samplers with time width shaping" in the block diagram in Fig. 3. The data consist of detection times and detection positions of all of the 7 PSD planes for an off-line analysis. The event filter selects a signal derived from single particle passages through 7 PSD layers. Such a selection is done by the PSD matrix coincidence system and only one hit events on a PSD layer are accepted. The event filter plays a role as a coincidence unit that selects events from the sampled signals and generates the information on the candidate muon path when the 2 signals of the counter are detected simultaneously on each PSD layer. This function is shown as "*X*-*Y* coincidence checker" in the block diagram. When two or more PSDs produce signals simultaneously and when only one signal is produced from each PSD, the path information is generated through the function "inter-plane coincidence checker". This decision logic is called the multiplicity cut selection (Tanaka et al., 2001). The path information consists of the number of PSDs that produced signals, 7 data sets containing the relative detection position differences from the first vertex point in the hodoscope for horizontal and vertical scintillator strips and timings. These data are read by the network processor and accessed by a data acquisition (DAQ) PC to download them. The time windows for both of "*X*-*Y* coincidence checker" and "inter-plane coincidence checker" are adjustable from 10 ns to 160 ns through a silicon transmission control protocol (SiTCP) utility software.

MURG12 requires an external memory device (such as a DAQ PC) because the size of the internal memory is too small (2088 kbit: 18 kbit (9 bit × 2 kword) × 116) to store

GID
3, 1–30, 2013

the data. The internal memory is used for register files of MURG12 and SiTCP, and only the real time data are temporary buffered in the FPGA. The time stamp of the data sets is therefore generated from a PC real-time clock (a clock that keeps track of the time even when the computer is turned off). These data are temporarily stored into a local hard disk drive in the DAQ-PC for various checks and are subsequently zipped and transferred to the remote terminal using a high-speed mobile phone network. Except for this part, no CPU and no other programmable sequencers are required. This design has advantages in terms of power consumption and operation failure rate. The measured power consumption of the readout module is 40 W. The antishower selection and histogram generation are done by an external PC at in this stage. The procedure is explained in the next paragraph.

As stated before, only events giving signals in all seven PSD are kept. Moreover, the recorded positions in the PSD need to be consistent with a straight line. For this, a histogram is filled with the angle of the incident particle, calculated from each pair of PSD in the detector (a total of combinatorics of 7 by 2, i.e. 21 entries). If the standard deviation of the obtained distribution is larger than a threshold value of 200 mrad, the event is discarded. The angular distribution of the events accepted by this selection is saved in the data stream. An angle of the incident particle is calculated using the difference between detection positions of each two PSDs. More in detail, if we label the PSDs #1, #2, #3, #4... from the upstream detector, an angle of the incident particle is calculated between #1 & #2, #2 & #3, and #3 & #4, and so on. The accidental muon rate is drastically reduced to a negligible level by making at least an octet coincidence in this system. If the deviation of the angle is larger than a given threshold level after comparing the incident angle between each two PSD layers, i.e. #1 & #2, #2 & #3, and #3 & #4, and so on, such an event is discarded. After the event selection, a histogram that shows the angular distribution of the event is generated.

GID
3, 1–30, 2013

3 Test measurement with the multi-PSD system

In order to confirm the feasibility of this technique, the multi-PSD system comprising 4 PSDs and MURG08 modules were used by Kusagaya et al. (2012) to image the parasitic cone and the adjacent craterlets formed in the 1910 eruption at the base of Usu volcano of which topographic sketch map is shown in Figs. 4 and 5. The detection system is located about 300 m east from the summit of the hill MS in the figure. Considering the speed limitations of MURG08 module, only 11 scintillator strips were used for each plane.

In this test measurement, the detection system consists of 88 scintillator strips to make an active area of 1.21 m^2 with an angular resolution of ±110 mrad (±55 mrad at 75 % coverage). The candidates for muon events were requested to satisfy the following conditions:

a. The number of hits in each PSD must be 1.

b. The track obtained in each PSD combination must be on a straight line within the angular threshold of 200 mrad (antishower selection).

c. The track obtained for each muon candidate must have penetrated rock with a thickness of at least 100 m.

Figure 6 shows the density distribution as obtained with the test measurement. The error includes the statistical errors at 1σ confidence level (CL) and the systematic errors that were estimated by two independent measurements using different combinations of scintillator strips. Because the geometrical acceptance becomes smaller for larger negative azimuth angles, error bars tend to be larger longer. The accuracy in the density measurement is ±2 % in 290 h for the maximum geometrical acceptance. The direction of the highest density coincides with that of the largest crater A. Although there are other two higher density regions for $\varphi = -330$ mrad and $\varphi = -600$ mrad, these anomalies are not statistically significant in the present measurement.

GID
3, 1–30, 2013

As shown in Fig. 6, the typical path length ranges from 500 to 1000 m for $\varphi < 50$ mrad, but it exceeds 1000 m for $\varphi > 500$ mrad. The lower density region can be seen for $\varphi < -660$ mrad. It is probably not because the density decreases, but because the signal to noise ratio increases. Based on this test measurement it was clarified that the BG rate with 4 PSDs are comparable to the muon penetration flux for 1000 m rock.

Tanaka et al. (2007) reported that the observation time to resolve the density structure of the similar sized target (Showa-shinzan lava dome in Fig. 4) was 4 months. Even though we consider the size of the detector they used was 1/3 of the present system (4000 cm^2), the imaging speed is improved by a factor of 3. The measured data transfer rate between MURG12 and the PC was 0.6 Gbit s^{-1} for the test system (4 PSD layers × 22 scintillator strips). This means that the rate from the full system (7 PSD layers × 28 scintillator strips) will be 1.3 Gbit s^{-1}. The rate of the events that hit 3 PSD layers and 4 PSD layers simultaneously is ∼ 26 000 h and ∼ 11 000 h, respectively after multiplicity cut selection but before non-linear cut selection. The difference in counting rate comes from the solid angle of the hodoscope.

4 Review of eruption activities of Usu volcano

In advance of the volcanological discussion of results of the test measurement, the volcanic activities of Usu volcano will be briefly reviewed.

A simplified topographic map of Usu volcano is shown in Fig. 4 that indicates several lava domes and upheavals (cryptodomes and mounds) in the summit crater and at the eastern and the northern bases. In the figure, HM (Higashi-Maruyama) may have similar origin to MS (Meiji-Shinzan) that shall be studied in the present paper while the origins of KP (Kompirayama) and NM (Nishi-Maruyama) have not been analytically established. Their formations were historically recorded at various accuracies, and their magmas were all dacitic. The two lava domes, Ko-Usu (small Usu) and Oo-Usu (big Usu) at the summit) were formed in 1822 and 1853, respectively. Their formations were legendarily recorded, but not scientifically. These summit lava domes may have

GID
3, 1–30, 2013

straightly derived from the magma reservoir, and may keep different subsurface structures from parasitic domes. Since 20th century, every event was observed by geophysical and geological methods of those days. It may be said that the activities of Usu volcano are manifestations of characteristics of dacitic magmas i.e. high viscosity. The recent four eruptions are briefly remarked as follows.

4.1 The 1910 eruption

More than 40 craterlets of small and large in diameter were produced at the northern base of Usu volcano roughly along the contour of 200 m a.s.l. They may be grouped into two, MS group and Kompira (KP) group, and an isolated one as shown in Fig. 4. In the MS area, the ground upheaved about 70 m forming a hill (named MS hill) that has been believed to be a "cryptodome" that is defined as an upheaval caused by viscous magmas at very shallow depths. At KP area, any deformations were not particularly reported. At that period, seismometers were operated at Sapporo, about 100 km distant, and a temporal seismic observation was carried out at the base of the volcano, and the routes of precise levels passed by the volcano. MS hill was named "Meiji-Shinzan" (the new mountain formed in Meiji era). Omori (1911–1913, 1920) left voluminous synthetic papers discussing explosions, earthquakes and deformations observed in the 1910 eruption.

4.2 The 1944 eruption

Before main activity of the lava dome formation for roughly 3 months, February to May, the ground at Yanagi-Hara village (YH in Fig. 4) had risen about 30 m, but no other surface phenomena, and upheaval apparently migrated about 1.5 km northward. At this point, the ground upheaved continuously and explosions began and the hot lava extruded the surface in November 1944. A dacitic lava dome extruded to a relative height of about 400 m in August 1945, about 15 months after the first sign of upheaval. Seismometric networks were temporarily operated around the volcano and precise

GID
3, 1–30, 2013

levels were repeated along a route passing by the doming site. The lava dome was named “Showa-Shinzan” (the new mountain formed in Showa era), abbreviated as SS in Fig. 4. Minakami, Ishikawa and Yagi (1951) gave a full detail of this eruption.

4.3 The 1977 eruption

Magmatic eruptions took place within the summit crater producing 20 vents in total for 14 months and were followed by continuous tilts of the summit part with incessant earthquakes for about 5 yr. Immediately after the commencement of this eruption, a volcano observatory was established at the northern base of the volcano by Hokkaido University and was equipped with telemetering systems of various kinds of signals. Yokoyama et al. (1981) reported the results of geophysical observations of this eruption. Later Yokoyama and Seino (2000) interpreted the three eruptions, in 1910, 1944 and 1977 from the standpoint of geophysical processes.

The 2000 eruption: firstly phreatomagmatic explosions outburst and later phreatic ones frequently occurred at the northwestern base forming more than 60 vents including small ones, and their activities were observed and discussed by members of various institutes. Their results were published in 27 papers on Bull. Volcanol. Soc. Japan (Vol. 47, 2002, in Japanese with English abstracts).

4.4 Muon radiography of the 1944 Usu domes

To the 1944 lava dome, Showa-Shinzan (SS in Fig. 4), muon radiography was already applied by Tanaka et al. (2007b) and the result was interpreted by Tanaka and Yokoyama (2008). The temporal sequence of the dome formation was visualized by the results of repeated precise levels (Minakami, 1947; Yokoyama, 2000): The top of magma branch was below the aquifer that ranged from 200 m b.s.l. to 100 m a.s.l., in June 1994, and the ground continued to upheave. In August, the magma contacted the aquifer causing explosions, and in November, the magma tip exposed itself at the summit of the mound. Thereafter the magma still continued to rise and simultaneously

GID
3, 1–30, 2013

expanded laterally forming a bulbous structure. In September 1945, finally SS lava dome had completed its upheaval of relative height of about 300 m, or about 110 m above the mound.

The muon radiography revealed the internal structure of the upper part of SS lava dome: the top of the dome taking a bulbous shape measuring about 300 m in diameter and narrowing downwards. The diameter of the uppermost part of the conduitis estimated at 100 ± 15 m at an elevation of 260 m a.s.l. and 50 ± 15 m at an elavatipn of 217 m a.s.l. Such a structure agrees with the results of deformation analyses (Tanaka and Yokoyama, 2008).

In the present study, muon radiography is applied to the area of the 1910 eruption, i.e. Meiji-Shinzan including MS hill and the area of several craterlets. The detectors were set at the Usu Volcano Observatory and aimed at the MS area, specifically A, B and C craterlets as shown in Fig. 5. The distances from the detectors to the targets ranged from 470 to 800 m.

5 Discussion

5.1 New findings on the 1910 eruption of Usu volcano from the present test measurement

The temporal sequence of the 1910 eruption is not clear because the volcano was located at a remote district at that time, and many explosive vents, small and large in diameter, opened at random in time and order, and their durations were relatively short. A temporal sequence of vent activity in the eruption provided by Omori (1913) is illustrated in Fig. 7 that contains some ambiguity according to the above reason. In the figure, the explosion diagram mainly indicates the periods of the first explosion of each craterlet, and each explosion did not continue for more than a few days. Some of the craterlets were reported to have repeated explosions. In Fig. 6, it is clear that the craterlets began their activities after the main seismic activities almost calmed. This

GID
3, 1–30, 2013

means that a few magma branches had been completed by this period and thereafter many sub-branches fed various craterlets. Sometimes strong magma branches such as A and B craterlets had formed upheavals on the ground surface.

5.1.1 a. MS hill (so-called cryptodome)

A simplified topographic sketch map around the MS triangulation point is shown in Fig. 5, originally surveyed in the scale of 1/5000 by the Geographical Survey Institute in the year 2000. After one century, small or shallow craterlets have faded or disappeared on the map. In Fig. 5, it is noticeable that MS hill itself is not located at the center of a parasitic cone measuring roughly 1 km in diameter on the northern slope of Usu volcano, and lacks the SW slope of the cone. In that part, there were several craterlets that repeated explosions in 1910, and the upper part of the parasite was not built conically. Here the main craterlets are labeled A, B and C in Fig. 5. We can find many photos of the explosions at these craterlets in the report of Omori (1911).

The topographies around the MS area are projected on north-south profile as shown in Fig. 8 where the original northern slope is assumed to be linear because we don't know exact topography before the 1910 eruption. In the 1910 eruption, the northern slope of the volcano entering into Lake Toya and measuring roughly 1 km long upheaved about 70 m at the maximum forming the MS hill.

Beneath the MS hill, no dense material is detected with the test measurement as shown in Fig. 8 (bottom). As for the underground conditions in this area, we remark the distribution of aquifers that should react with extruding magmas. Well (GSH-1) was drilled at the western base of Nishi Maruyama (NM hill) in 1970 (Fig. 4). If the present aquifer is assumed to be the same as in 1910, its bottom may be roughly 100 m b.s.l. as shown in Fig. 8 (top). If the magma head beneath MS hill contact with the aquifer, an explosive activity should occur. No explosive activity around the top of MS means that the magma head had remained deeper than 100 m b.s.l. This interpretation agrees with that the muon radiography does not detect any dens material at a shallow depth. MS point had upheaved about 70 m and the deformed area including MS is roughly 1 km

GID
3, 1–30, 2013

in basal diameter on the northern slope of Usu volcano (Figs. 4 and 5). In fact, the true center of the upheaval should be located at the area of A and B craterlets, and their explosions obstructed upheaval of the area. If MS were the peak of the upheaval caused by magmatic forces, we should observe dense material beneath it by the muon radiography. As a result, MS hill is not a cryptodome but a volcanogenetic mound.

5.1.2 b. Craterlet A

This is the biggest craterlet of this group still having a depth of about 43 m, as of the year 1910 and about 32 m in the year 2000. This magma body should have reacted with the aquifer causing violent phreatic explosions. This picture is consistent with a relatively narrow (50 m in diameter) high density anomaly that was found just beneath the craterlet in the direction of Craterlet A in Fig. 8 (bottom).

If a simple dilatation model is adopted to explain the formation of a large MS cone, the rising magma branch beneath craterlet A should be most probable as the pressure source.

5.1.3 c. Craterlet B

Its maximum relative depth is about 12 m as of the year 2000. The muon image shows statistically insignificant but some implication of dense material just below the craterlet as shown in Fig. 6. This craterlet may have exploded by reactions with the aquifer as well as craterlet A.

5.1.4 d. Craterlet C

It is a shallow craterlet measuring about 8 m in relative depth as of the year 2000. Below this craterlet, no exits dense material: probably a thin conduit issued phreatic material and exploded the surrounding ground. This is also consistent with our result that no clear density anomaly was found beneath Craterlet C.

GID
3, 1–30, 2013

As a result, in the area covering the craterlets, upheavals due to magmatic pressure acting mainly beneath craterlets A and B may have been partly obstructed by explosive activities of all the craterlets.

5.1.5 e. Gravity anomalies

The Bouguer gravity anomalies observed in a limited area of the MS area are shown in Fig. 9 where altitudes of the gravity points were determined by levelings (solid circles) and a barometer (hollow circles). Topographic corrections are not added because the points concerned are in a narrow area. High anomalies roughly predominate at the craterlet zone and qualitatively suggest the existence of dense magmatic material beneath the craterlets.

5.2 Multilayer high-speed muon radiography to reveal three stages of the magma intrusions at the base of Usu volcano

As future targets of muon radiography, we may group the magma intrusions on Usu volcano into three classes according to their intrusive depths and the surface phenomena.

5.2.1 a. Yanagi-Hara (YH) upheaval in 1944

An example of volcanogenetic deformation of similar dimension to the upheaval of MS hill, but not accompanied with eruptions, shall be remarked; It occurred at Yanagi-Hara village, south of SS dome, roughly 4 months earlier than the start of formation of the SS dome. It is labeled YH in Fig. 4 and its deformation curves are shown in Fig. 10 after Inoue (1948).

The benchmarks were on the railroad passing in the north-south direction roughly parallel to River Osaru (Fig. 4) and the YH point measuring height of about 43 m a.s.l. before the 1944 eruption had upheaved about 23 m in about 3 months (February to April, 1944) as shown in Fig. 9. The maximum upheaval in this area was estimated at

GID
3, 1–30, 2013

about 30 m outside the railroad. This upheaval was not accompanied with any explosive or fumarolic activities, and the deformation activity apparently migrated about 1.5 km northward after March, and actually another magma branch intruded at the new spot where Showa-Shinzan (SS) lava dome was formed by explosions and upheavals in about 15 months. The magma branch acted at YH was different from that resulted in SS dome because the dacitic magmas are viscous and cannot easily move horizontally, and furthermore, the active periods of YH and SS events were partly overlapped each other. For the YH event, we can refer the aquifer observed at well (GS-R1, Fig. 4) drilled in 1966. Its bottom is about 160 m b.s.l. At YH, the magma top may have remained at a depth of deeper than (43 + 200 =) 243 m. The magma branch could upheave the ground 30 m in three months but did not contact the aquifer. The YH upheaval is a volcanogenetic mound, and the magma may have remained at a depth of over 300 m.

5.2.2 b. MS hill in 1910 (Meiji-Shinzan)

Below craterlets A and B, the magma branched from the main conduit of Usu volcano rose up upheaving the ground and further contacted the aquifer at a depth of about 100 m b.s.l. causing phreatic explosions. Many magma branches provoked similar explosions producing many craterlets as shown in Fig. 22, but each activity continued for rather short time. This means that the magma branches were not so voluminous. Magmas themselves could not extrude above the ground surface.

5.2.3 c. SS lava dome in 1944 (Showa-Shinzan)

The magma branch originating SS lava dome passed through the above two stages successively. The magma finally extruded above the mound forming SS lava dome.

The latter two stages (b and c) were verified by muon radiography. In the near future, by applying multilayer high-speed muon radiography to YH upheaval, a complete picture of three stages of the magma intrusions on Usu volcano will be obtained.

GID
3, 1–30, 2013

6 Conclusions

The present system requires an external DAQ computer to store event by event data. Therefore, the total power consumption of the readout module exceeds 80 W. However, if the following parameters are fixed, event by event data will no longer have to be saved, and only histogram data and values of event counters will be generated in an internal memory of the FPGA by employing the same processing method as MURG08: (a) the number of PSD layers and (b) antishower selection criteria. In the future work on Usu Volcano, the number of PSD layers will be optimized as a function of the size of the target.

By comparing with the prior study by Tanaka et al. (2007), we confirmed that the multilayer PSD system with MURG08 improved that the imaging speed by a factor of 3 even with the relatively high operation failure rate. By employing a hardware-based MURG12, this speed will be further improved.

By the muon radiographic survey of MS mound, it was clarified that a magma branch below A craterlet rose to a depth of about 100 m a.s.l. and reacted with the aquifer causing explosions. At the base of Usu volcano, we know the three stages of magma extrusions; First, the magma stopped below YH mound, second the magma reached the aquifer beneath MS craterlets, and third, the magma extruded over the ground at SS lava dome. The latter twos were verified by the muon radiography, and the authors expect that subsurface structure of the YH mound should be also clarified by muon radiographic imagings.

Acknowledgements. This work is a part of a collaborative research with T. Kusagaya, A. Taketa, T. Uchida, M. Tanaka, H. Oshima and T. Maekawa. The authors acknowledge them for valuable collaboration. S. Okubo is also acknowledged for valuable discussions. Special funding arrangements by related people of ERI and MEXT are acknowledged. The manuscript greatly benefited from the useful comments provided by C. Carloganu.

GID

3, 1–30, 2013

References

Alvarez, L. W., Anderson, J. A., Bedwei, F. E., Burkhard, J., Fakhry, A., Girgis, A., Goneid, A., Hassan, F., Iverson, D., Lynch, G., Miligy, Z., Mousaa, A. H., Sharkawi, M., and Yazolinio, L.: Search for hidden chambers in the pyramids, Science, 167, 832–839, 1970.

George, E. P.: Cosmic rays measure overburden of tunnel, Commonwealth Engineer, 455–457, 1955.

Inoue, W.: A research report on seismicity and deformation related to the 1944 activity of Usu volcano, Bull. Seismolo. Observ., JMA, 14, 9–24, 1948 (in Japanese).

Lesparre, N., Gibert, D., Marteau, J., Komorowski J., Nicolin, F., Coutant, O., Density muon radiography of La Soufrie're of Guadeloupe volcano: comparison with geological, electrical resistivity and gravity data, Geophys. J. Int., 190, doi:10.1111/j.1365-246X.2012.05546.x, in press, 2012.

Minakami, T.: Recent activituies of volcano Usu (1), Bull. Earthq. Res. Inst., 25, 65–69, 1947.

Minakami, T., Ishikawa, T., and Yagi, K.: The 1944 eruption of volcano Usu in Hokkaidu, Japan. Bull. Volcanolo., 11, 45–157, 1951.

Omori, F.: The Usu-san eruption and earthquake and elevation phenomena, Bull. Imp. Earthq. Inv. Com., 5, 1–137, 1911.

Tanaka, H., Nagamine, K., Kawamura, N., Nakamura, S. N., Ishida, K., and Shimomura, K.: Development of the cosmic-ray muon detection system for probing internal-structure of a volcano, Hyperfine Interact., 138 521–526, 2001.

Tanaka, H. K. M., Nakano, T., Takahashi, S., Yoshida, J., Takeo, M., Oikawa, J., Ohminato, T., Aoki, Y., Koyama, E., Tsuji, H., and Niwa, K.: High resolution imaging in the inhomogeneous crust with cosmic ray muon radiography: The density structure below the volcanic crater floor of Mt. Asama, Japan, Earth Planet. Sci. Lett., 263, 104–113, 2007a.

Tanaka, H. K. M., Nakano, T., Takahashi, S., Yoshida, J., Ohshima, H., Maekawa, T., Watanabe, H., and Niwa, K.: Imaging the conduit size of the dome with cosmic ray muons: The structure beneath Showa Shinzan Lava Dome, Japan Geophys. Res. Lett., 34, L22311, doi:10.1029/2007GL031389, 2007b.

Tanaka, H. K. M. and Yokoyama, I.: Muon radiography and deformation analysis of the lava dome formed by the 1944 eruption of Usu, Hokkaido – Contact between high-energy physics and volcano physics, Proc. Jpn. Acad. Ser. B, 84, 107–116, 2008.

GID
3, 1–30, 2013

Tanaka, H. K. M., Nakano, T., Takahashi, S., Yoshida, J., Takeo, M., Oikawa, J., Ohminato, T., Aoki, Y., Koyama, E., Tsuji, H., Ohshima, H., Maekawa, T., Watanabe, H., and Niwa, K. Radiographic imaging below a volcanic crater floor with cosmic-ray muons, Am. J. Sci., 308, 843-850, 2008.

Tanaka, H. K. M., Uchida, T., Tanaka, M., Takeo, M., Oikawa, J., Ohminato, T., Aoki, Y., Koyama, E., and Tsuji H.: Detecting a mass change inside a volcano by cosmic-ray muon radiography (muography): First results from measurements at Asama volcano, Japan, Geophys. Res. Lett., 36, L17302, doi:10.1029/2009GL039448, 2009a.

Tanaka, H. K. M., Uchida, T., Tanaka, M., Shinohara, H., and Taira, H.: Cosmic-ray muon imaging of magma in a conduit: Degassing process of Satsuma-Iwojima Volcano, Japan, Geophys. Res. Lett., 36, L01304, doi:10.1029/2008GL036451, 2009b.

Uchida, T., Tanaka, H. K. M., and Tanaka, M.: Space Saving and Power Ef?cient Readout System for Cosmic-Ray Muon Radiography, IEEE T. Nuclear Sci., 56, 448–452, 2009.

Yokoyama, I.: The formation of cryptodomes: Usu volcano, Hokkaido, Japan, Bull. Volcanol. Soc. Jpn., 47, 151–160, 2002 (in Japanese with English abstract).

Yokoyama, I. and Seino, M.: Geophysical comparison of the three eruptions in the 20th century of Usu volcano, Japan. Earth Plan. Space, 52, 73–89, 2000.

Yokoyama, I., Yamashita, H., Watanabe, H., and Okada, Hm.: Geophysical characteristics of dacite volcanism – The 1977-1978 eruption of Usu volcano, J. Volcanol. Geotherm. Res., 9, 335–358, 1981.

GID

3, 1–30, 2013

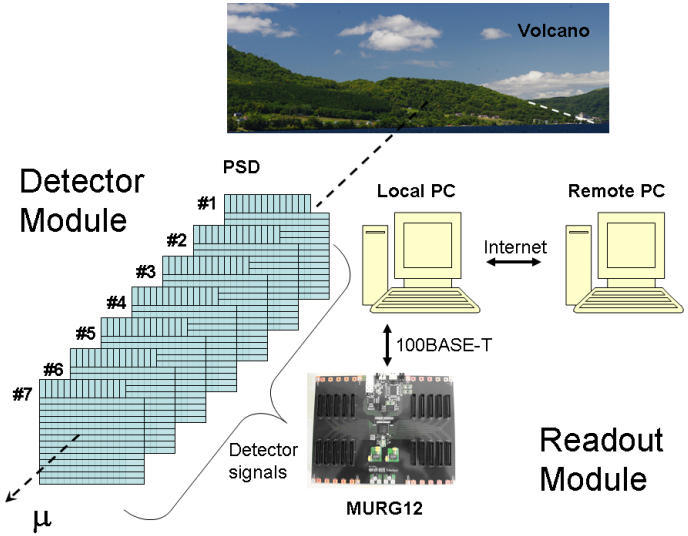

Fig. 1. Diagram of the observation system for multilayer muon high-speed radiography.

GID
3, 1–30, 2013

Multilayer muon high-speed radiography

H. K. M. Tanaka and I. Yokoyama

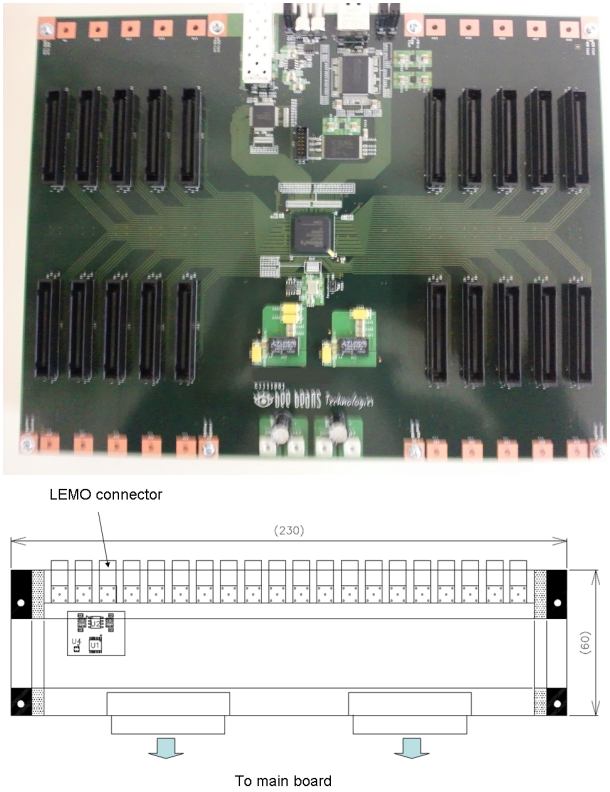

Fig. 2. Photograph of the main board of MURG12 (upper) and the schematic side view of the daughter board (lower). U1 is for low voltage differential signaling. U2 is the low capacitance transient voltage suppression (TVS) array. U4 is the low capacitance electrostatic-discharge-(ESD) protection diode array.

GID
3, 1–30, 2013

Multilayer muon high-speed radiography

H. K. M. Tanaka and I. Yokoyama

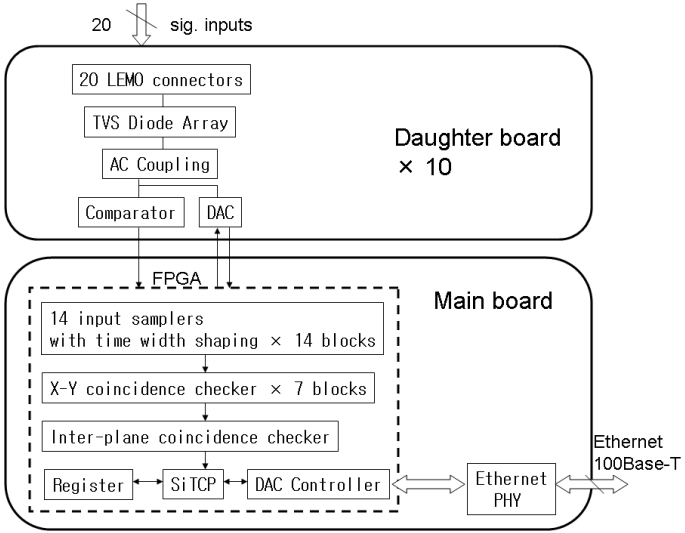

Fig. 3. Block diagram of MURG12.

GID
3, 1–30, 2013

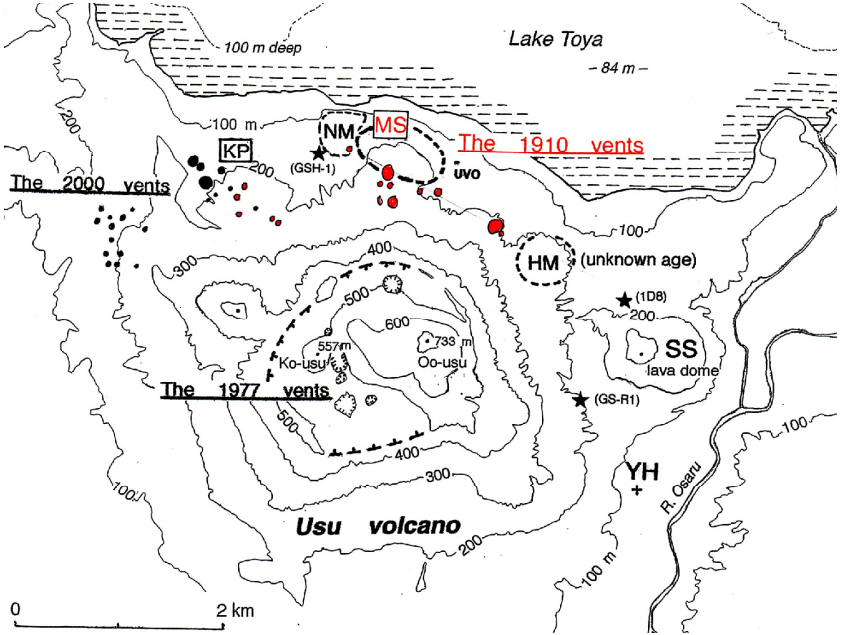

Fig. 4. Topographic sketch map of Usu volcano. KP: Kompira craterlet group, MS: Meiji-Shinzan craterlet group, SS: Showa-Shinzan lava dome , YH: Yanagi-Hara mound. Muon detection system is placed at UVO: Usu Volcano Observatory in this map.

GID
3, 1–30, 2013

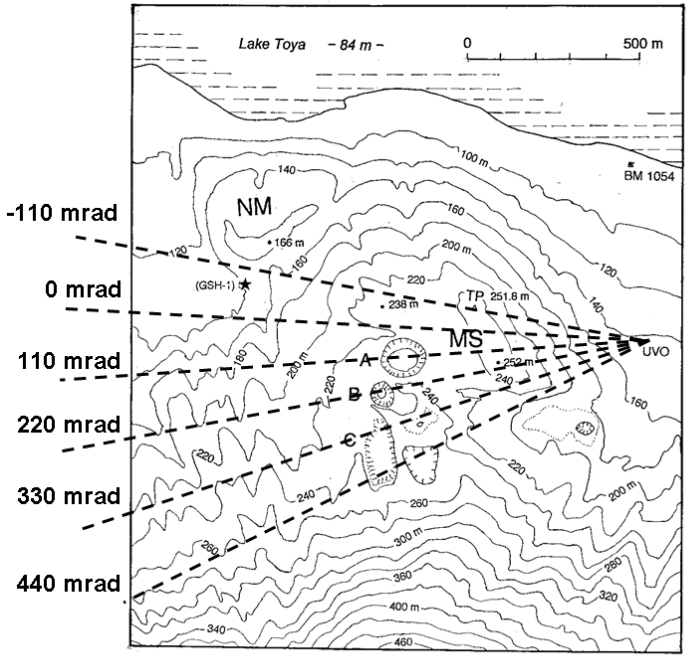

Fig. 5. Topographic sketch map of the MS area as of the year 2000, originally surveyed by the Geographical Survey Institute in the scale of 1/5000. A, B and C denote the craterlets muon radiographically surveyed in the present paper. NM is Nishi-Maruyama, unknown its origin.

GID
3, 1–30, 2013

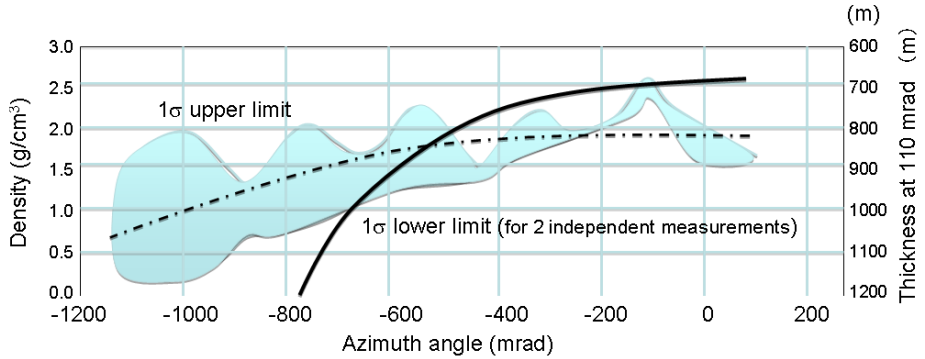

Fig. 6. Density distribution of 1910 MS mound as a function of azimuth angle. The 1σ upper and lower limits for the measurement is shown in the blue region. The broken line shows the result of taking moving average of the density distribution. The solid line indicates the thickness of the target at an elevation of 110 mrad.

GID
3, 1–30, 2013

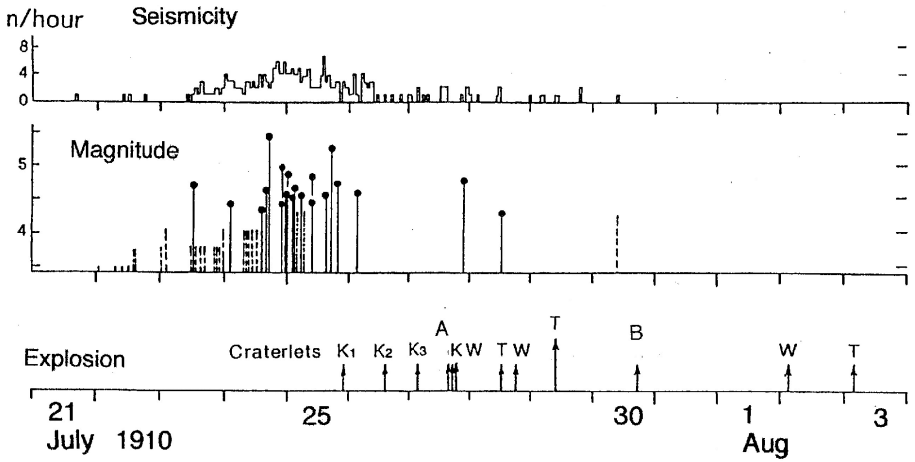

Fig. 7. Temporal sequences of the 1910 eruption of Usu volcano (after Yokoyama and Seino, 2000). Seismicity: hourly numbers of earthquakes ($M \geq 3.0$) observed at Sapporo. Explosion: strength in arbitrary scale. Craterlets K: Kompira group.

GID
3, 1–30, 2013

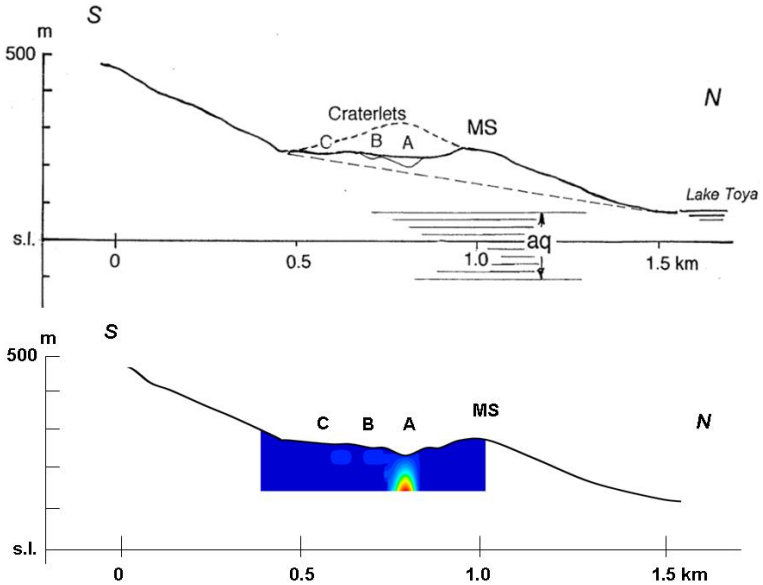

Fig. 8. A topographic profile in a south-north direction passing MS hill and the craterlets. "aq" indicates the aquifer observed at well GSH-1 (Fig. 5) (upper). Density projection as calculated from the result of muon radiography (lower).

GID
3, 1–30, 2013

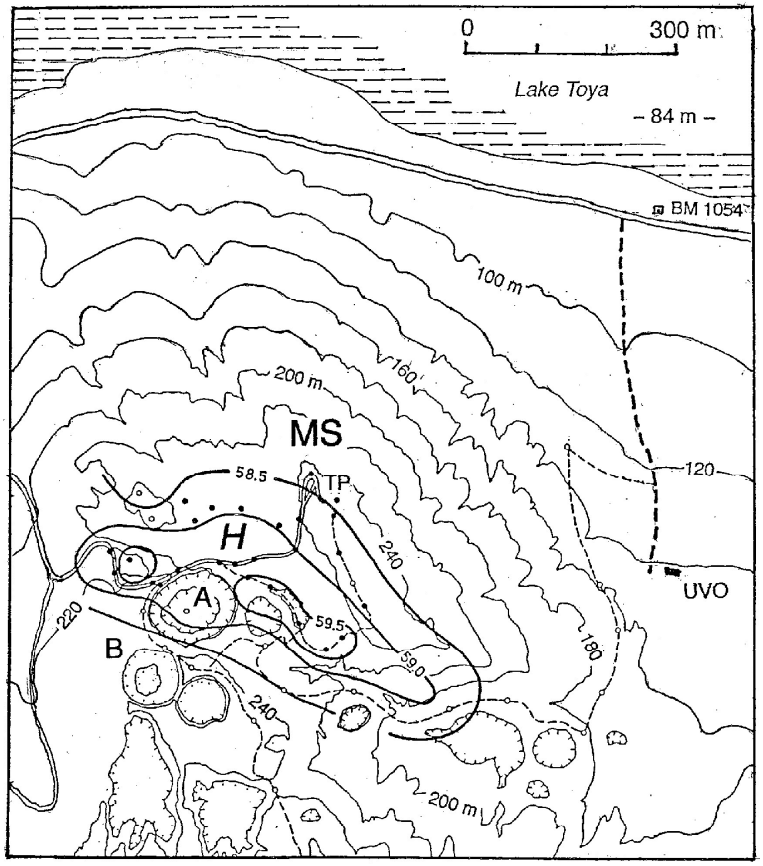

Fig. 9. Bouguer gravity anomalies in mgal around MS hill. High anomaly is predominant.

GID
3, 1–30, 2013

Multilayer muon high-speed radiography

H. K. M. Tanaka and I. Yokoyama

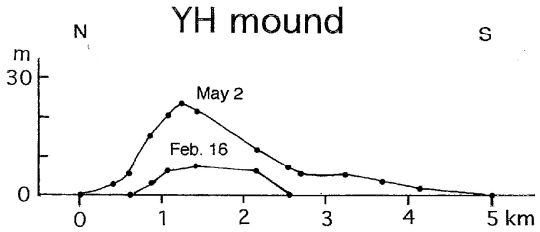

Fig. 10. Upheavals of YH (Yanagi-Hara) in 1944 (after Inoue, 1948).

GID
3, 1–30, 2013